Identification of the hygro-thermo-chemical-mechanical model parameters of concrete through inverse analysis

Massimiliano Bocciarelli[1]*, Gianluca Ranzi[2]

[1] Architecture, Built environment and Construction engineering Department, Politecnico di Milano (Technical University), Italy

[2] School of Civil Engineering, The University of Sydney, Australia

* Corresponding Author. E-mail: massimiliano.bocciarelli@polimi.it

Abstract

A wide range of parameters is required in input when applying hygro-thermo-chemical-mechanical models to concrete components with the aim of determining the variations over time of temperature, relative humidity and shrinkage induced deformations. While a sub-set of these material parameters can be evaluated on the basis of the concrete mix specifications or from literature data, this paper presents a robust inverse analysis procedure for the identification of the remaining sub-set of parameters that are characterised by a large variability and, in some cases, do not have a precise physical meaning and are not amenable to a direct measurement. The particularity of this paper is to propose different strategies for the characterisation of these material parameters that account for the presence of different exposure conditions, as these affect the outcomes and requirements of the parameter identification procedure. After introducing the adopted hygro-thermo-chemical-mechanical model, representative results of an extensive sensitivity analysis are presented in the first part of the paper to give insight into most effective number, location and duration of measurements to be used in input of the inverse analysis. The inverse analysis procedure is then presented and applied to a number of selected scenarios to highlight its robustness considering different boundary conditions in terms of external temperature and relative humidity surrounding the concrete. The ability to characterise these parameters will support a wider use of these hygro-thermo-chemical-mechanical models, especially for those applications in which humidity and temperature profiles significantly influence the structural response, for example when predicting curling in industrial pavements and non-uniform shrinkage profiles in composite steel-concrete slabs.

Keywords

Concrete; inverse analysis; long-term behaviour; moisture diffusion; sensitivity analysis; shrinkage.

1. Introduction

Concrete structures are significantly influenced by the time-dependent behaviour of the concrete that affects their serviceability and durability. An inaccurate evaluation of this service response can lead to undesired excessive deformations and occurrence of cracking. Concrete time effects are significantly dependent on the moisture transport and heat transfer mechanisms that take place in the concrete and that control, for example, the hardening process, water release, cement hydration, and volume changes. Different numerical and experimental studies are available in the literature that deal with the concrete behaviour, especially considering its early age. Bažant and Najjar [1] presented a material model capable of describing the nonlinear moisture transport that takes place in concrete. Several researchers extended this approach in following years, for example, by incorporating a thermodynamics based approach for the cement hydration [2] or by establishing a thermo-chemo-mechanical model to account for the aging effect on strength development and the micro-scale description of the material [3-5]. Other recent contributions considered the influence of cracking on the permeability [6] or included a sink term into the diffusive moisture equation to capture the internal water consumption occurring during cement hydration [7,8]. The use of an enhanced cement hydration model was presented in [9] while the influence of the meso-structure was investigated in [10-12]. A hygro-thermo-chemical model that accounted for the effect of cement hydration on both moisture and temperature calculations was considered in [13,14]. The mechanical coupling is usually based on a linear relationship between the variations over time of the relative humidity and the consequent free shrinkage deformations (see, e.g. [13,14,15,16]).

The use of these models is particularly relevant in applications where the effect of shrinkage induced deformations are important, such as curling in industrial pavements [17,18] and shrinkage gradients in composite floor systems [19-22] (where the presence of different exposure conditions, due to the presence of subgrade/waterproofing membrane and profiled steel sheeting, respectively, influence the mechanical response). In the latter case, the occurrence of the non-

uniform shrinkage profiles has been only recently identified [19] and the ability to couple the hygro-thermo-chemical behaviour to its mechanical response will enable more accurate structural predictions associated to the serviceability limit state requirements of building floors. For these applications, the wider use of hygro-thermo-chemical-mechanical models for service design and modelling needs to be supported by techniques capable of adequately identifying the required material parameters, especially in applications where they can give useful insight into the structural problem. Not all material parameters to be specified in input in these hygro-thermo-chemical-mechanical models can be easily determined and, to better highlight this aspect, the model material parameters are subdivided into the following two sets: (i) one set of parameters that can be evaluated based on the concrete mix specifications or from data reported in the literature; and (ii) a second set of parameters characterised by a large variability (based on data available in the literature) and, among these, many parameters do not possess a precise physical meaning and, for this reason, are not amenable to a direct measurement.

In this context, the main contribution of this paper relies on the development of a robust inverse analysis procedure for the identification of the second set of material parameters (i.e. listed at point (ii) above) that are required in input for the use of the hygro-thermo-chemical-mechanical models. This paper contributes to this effort by proposing different strategies for the characterisation of the material parameters considering different exposure conditions.

In this work, the robustness of the proposed inverse analysis procedure is determined based on the use of pseudo-experimental results as input data (e.g. [23-25]) that includes measurements of temperature, relative humidity and total deformations. This data has been generated considering the same exposure conditions of commonly available reinforced or prestressed concrete slabs, i.e. exposed on both its surfaces, and of slabs exposed only from one side because sealed on its opposite side (e.g. composite slabs and industrial pavements). The proposed methodology is developed with the idea of minimising the number and the duration of the measurements to be carried out and of investigating how these are influenced by different

exposure conditions. After introducing the key features of the hygro-thermo-chemical-mechanical model considered in this study, the main outcomes and representative results obtained from an extensive sensitivity analysis are presented because providing insight into the most effective number, location and duration of the measurements to be used as input of the inverse analysis procedure. The basis of the inverse analysis procedure is then presented and its robustness is tested against selected scenarios constructed using pseudo-experimental data subjected to different degrees of noise and for different external temperatures and relative humidities surrounding the concrete. Representative results are reported in the paper to give insight into the use and effectiveness of the proposed methodology. These results are also expected to support the effective planning of the instrumentation setup to be used in experimental tests on service conditions performed in controlled laboratory environments and for the arrangement of in-situ monitoring and investigations, for example during construction or during day-to-day service operations, associated to applications whose service response is influenced by shrinkage.

2. Hygro-thermo-chemical-mechanical model

The hygro-thermo-chemical-mechanical model considered in this paper is able to predict the variations of the relative humidity *h*, temperature *T* and deformation ε that take place over time within the spatial domain Ω of a concrete component taking into account its environmental conditions. The model here presented has been proposed in [13] and applied to a concrete mix without the presence of silica fume. The main features of the model and its numerical implementation are described in the following.

The principal chemical reaction occurring during hardening of a concrete mix is cement hydration, whose extent is here expressed through a scalar variable α_c, computed as the ratio between the actual level of hydration X_c and its theoretical asymptotic value $X_c^{\infty,th}$ achievable

under ideal hygro-thermal conditions. The maximum level of the reaction degree $\alpha_c^\infty = X_c^\infty / X_c^{\infty,th}$ is usually smaller than one, i.e. $\alpha_c^\infty < 1$. According to [26], we may assume $\alpha_c^\infty = (1.032\, w/c)/(0.194 + w/c)$, in which *w/c* depicts the water-to-cement ratio. The variation over time $\dot{\alpha}_c$ increases with relative humidity content and reduces while approaching its asymptotic value α_c^∞ as expressed by the following Arrhenius type equation:

$$\dot{\alpha}_c = \frac{A_{c1}\left(A_{c2}/\alpha_c^\infty + \alpha_c\right)\left(\alpha_c^\infty - \alpha_c\right)e^{\left(-\eta_c \alpha_c/\alpha_c^\infty\right)}}{\left[1+(a-ah)^b\right]} \cdot e^{\left(-\gamma_c/T\right)} \tag{1}$$

where $\gamma_c = E_{ac}/R$, E_{ac} is the hydration activation energy and *R* represents the universal gas constant. Parameters A_{c1}, A_{c2} and η_c have no precise physical meaning and govern the so-called normalized chemical affinity. The function $b_h(h) = \left[1+(a-ah)^b\right]^{-1}$ takes into account the slowing of the hydration process when relative humidity decreases below a certain value (around 80%). Parameters *a* and *b* are usually taken equal to 7.5 and 4.0, respectively, (see [1]).

The total water content *w*, present in the concrete mix, is expressed as the sum of the evaporable water w_e and the non-evaporable water w_n, the latter being the water chemically bonded by cement hydration and expressed as $w_n(\alpha_c) = k_c \alpha_c c$, with *c* being the cement ratio content and k_c a material parameter that, according to [13] and references herein, can be assumed equal to 0.253. The evaporable water is expressed as a function of the relative humidity (sorption isotherm curve) and of the degree of cement hydration α_c as follows:

$$w_e(h,\alpha_c) = \kappa_{vg}^c \alpha_c c\left(1-1/\overline{e}_2\right) + \left[w_0 - 0.188\alpha_c c - \kappa_{vg}^c \alpha_c c\left(1-1/\overline{e}_1\right)\right] \cdot \frac{\overline{e}_2 - 1}{\overline{e}_1 - 1} \tag{2}$$

124 in which w_0 $\left(=(w/c)c\right)$ is the initial water content and it is assumed that $\overline{e}_2 = e^{10\left(g_1\alpha_c^\infty - \alpha_c\right)h}$

125 and $\overline{e}_1 = e^{10\left(g_1\alpha_c^\infty - \alpha_c\right)}$. Equation (2) also depends on material parameters κ_{vg}^c and g_1 that

126 govern the amount of water contained in the cement gel pores and the shape of the sorption curve,

127 respectively.

128 Starting from the consideration that $w = w_e(h,\alpha_c) + w_n(\alpha_c)$, the variation of the humidity field

129 over time and space is described by the combination of the Fick's law, expressing the flux of

130 water mass **j** as proportional to the gradient of the relative humidity *h* (i.e. $\mathbf{j} = -D_h \nabla h$) and the

131 water mass balance equation, e.g. [1,13]:

$$\frac{\partial w_e}{\partial h}\frac{\partial h}{\partial t} = \nabla\cdot\left[D_h\nabla h\right] - \left(\frac{\partial w_e}{\partial \alpha_c} + \frac{\partial w_n}{\partial \alpha_c}\right)\dot{\alpha}_c \qquad \text{in } \Omega \tag{3}$$

132 In the above equation, the moisture permeability D_h depends on the relative humidity *h* and

133 temperature *T* as per the following expression [13,27]:

$$D_h(h,T) = \frac{D_1}{\left[1+\left(D_1/D_0-1\right)\left(1-h\right)^n\right]}\cdot \mathrm{e}^{\left(E_{ad}/RT_0 - E_{ad}/RT\right)} \tag{4}$$

134 in which T_0 is the reference room temperature (assumed equal to 296°*K*), $E_{ad}/R = 4700K$ (see

135 e.g. [1]), and parameters D_0, D_1 and *n* depend on the specific concrete mix.

136 The temperature field is described by the combination of the Fourier's law, expressing the heat

137 flux **q** as a function of the temperature spatial gradient $(\mathbf{q} = \lambda\nabla T)$, and the enthalpy balance

138 equation as follows:

$$\rho c_t \frac{\partial T}{\partial t} = \nabla\cdot\left[\lambda\nabla T\right] + Q\dot{\alpha}_c \qquad \text{in } \Omega \tag{5}$$

where T is the absolute temperature, λ is the heat conductivity assumed constant in the present study, ρ and c_t depict the concrete mass density and the specific heat, respectively, and $\dot{Q}_c$ represents the rate of heat generated by cement hydration, calculated as $\dot{Q}_c = \dot{\alpha}_c c Q_c^{\infty}$, with Q_c^{∞} being the total heat content per unit cement mass.

Equations (3) and (5) are coupled by their dependency on the degree of cement hydration α_c as well as by the moisture diffusion coefficient D_h that depends on both temperature and relative humidity.

The relative humidity obtained with the hygro-thermo-chemical model is then associated to a free shrinkage hydrostatic strain tensor by means of the following expression:

$$\dot{\varepsilon}_{sh} = k_{sh} \dot{h} \tag{6}$$

which defines a linear relationship between the rate of change over time of the free shrinkage deformation $\dot{\varepsilon}_{sh}$ and the corresponding rate of change of the relative humidity $\dot{h}$ by means of the coefficient k_{sh}. The value for k_{sh} is usually considered to remain constant for practical applications (e.g. [6,15,28,29]) even if, in reality, it has been shown that its value varies with the relative humidity, e.g. [16,30]. Values reported in literature for k_{sh} exhibit a large scatter, ranging between 5×10^{-4} and 3.5×10^{-3} (e.g. [29,31]) and, because of this, the value for k_{sh} needs to be calibrated for different concrete mixes. By performing a time integration of Equation (6), the free shrinkage deformation can be expressed as:

$$\varepsilon_{sh}(t) = k_{sh}\left(h(t) - h(0)\right) \tag{7}$$

The hygro-thermo-chemical-mechanical relationships introduced in Equations (1-7) depend on many parameters. Some of them, listed in the upper part of Table 1, can be evaluated based on the concrete mix specifications or from well-known data reported in the literature. Other parameters are affected by a large variability and, among these, some do not possess a precise

physical meaning. This set of parameters is reported in the lower part of Table 1 and their range of variation (obtained and derived from [13,14,31,32]) is collected in Table 2.

The numerical solution of the proposed hygro-thermo-chemical model is achieved with the finite element method by solving the following discretized equations:

$$\begin{cases} \mathbf{W}\dot{\mathbf{H}} + \mathbf{D}\mathbf{H} = \mathbf{F} \\ \mathbf{C}\dot{\mathbf{T}} + \mathbf{\Lambda}\mathbf{T} = \mathbf{Q} \end{cases} \tag{8}$$

where **H** and **T** depict unknown vectors that collect all nodal values (of the finite element discretization) of the relative humidity and temperature fields at each instant, while the system matrices are defined in Appendix A. The Dirichlet's boundary conditions (on *h* and *T*) are directly enforced on the vectors **H** and **T**, while Cauchy's boundary conditions enter into the right end side of the equation, see [33]. The system described in Equation (8) is solved by applying an explicit algorithm based on the θ-method [33,34].

The mechanical analysis of the problem is then carried out using standard structural analysis procedures. In particular, for the purpose of the simulations presented in this paper a time-dependent cross-sectional analysis is performed to account for the shrinkage effects evaluated with Equation (7) based on method of analysis widely accepted in the literature, e.g. [35].

The use of the proposed numerical model is illustrated in the following considering an unreinforced and unloaded concrete component with the following boundary conditions: (i) heat exchange can take place from its opposite surfaces; and (ii) two different sets of boundary conditions are considered for the relative humidity, i.e. one with both concrete surfaces exposed for drying (Figure 1a) and a second with only one surface exposed to dry and opposite surface sealed (Figure 1b). For ease of reference, these boundary conditions have been referred to as EE and ES, respectively, in Figure 1.

Representative results related to the humidity profiles are provided in Figures 2 and 3 at different time increments for a period of 10 years and considering two concrete thicknesses, namely

100 mm and 250 mm. The adopted concrete mix is typical of a normal-strength concrete and its specifications are presented in Table 3. The simulations have been performed considering two boundary conditions, i.e. exposed-exposed (Figure 1a) in Figures 2a and 3a as well as exposed-sealed (Figure 1b) in Figures 2b and 3b, and the model parameters are based on the mean values of the ranges included in Table 2 and on the values specified in Table 3. Results presented in Figures 2 and 3 have been calculated assuming a wet curing period of 10 days.

The results of Figures 2 and 3 highlight the ability of this model to simulate the highly nonlinear humidity profiles that can develop through the concrete thickness and how these can be influenced by the drying mechanism activated by the different external environmental conditions. In particular, the nonlinear variations of relative humidity illustrated in Figure 2 show that, when exposed to a dry environment (i.e. environmental relative humidity of 40%), the thin concrete component cannot approach an equilibrium condition through its entire thickness with the ambient conditions even after nearly 10 years from casting. In the case of the concrete component subjected to exposed-sealed environmental conditions, non-symmetric humidity distributions develop due to the inability of the concrete to dry from its sealed surface as shown in Figures 2b and 3b. For a thicker concrete component the moisture transport process is slower and requires more time than a thinner one in achieving a stationary solution. For example, after ten years of simulation the variation of relative humidity measured at mid height is smaller (Figure 3) than that occurring in the thinner specimen (Figure 2).

The corresponding free shrinkage profiles are determined by inserting the relative humidity distributions of Figures 2 and 3 into Equation (7) as shown in Figures 4 and 5 for thicknesses of 100 mm and 250 mm, respectively. The consequent total deformations are then evaluated from a time-dependent cross-sectional analysis based on the calculated free shrinkage profiles (dot lines in Figures 4 and 5), widely used in the literature for the evaluation of the service response of concrete structures (e.g. [35]) and their variations (i.e. of calculated total deformations) are

208 also plotted in Figures 4 and 5 at different instants in time (see continuous lines). From a
209 qualitative viewpoint, the total deformations induced in an exposed-exposed unreinforced
210 concrete component by the nonlinear shrinkage are constant through its thickness and well reflect
211 the simplifying assumption adopted in international concrete codes (e.g. [36,37]) that specify the
212 use of a constant shrinkage distribution for design purposes. In the case of an exposed-sealed
213 concrete component, the total deformations produced by the calculated humidity profile lead to
214 the development of a non-uniform shrinkage distribution. This behaviour is typical of industrial
215 pavements that can dry predominantly from their exposed upper surface (see e.g. [17,18]) and,
216 as recently reported in the literature, of composite floor systems in which concrete slabs are cast
217 on profiled steel sheeting and can only dry from the exposed surface (see e.g. [19,20,21,22]). As
218 expected, free shrinkage and total deformations are larger when considering thinner components,
219 as noted comparing Figures 4 and 5.

220 ## 3. Sensitivity analysis

221 The sensitivity analysis is intended to compute the influence of each sought parameter on the
222 measurable quantities and to support the design of the experiments for inverse analysis purposes.
223 In particular, the sensitivity analysis is applied to gain a better understanding on how the sought
224 material parameters, i.e. those listed in the lower part of Table 1, influence the variations of the
225 total deformations over time in order to assist the selection of the most effective time duration
226 and spatial positions to be considered for the proposed inverse analysis (see e.g., [25], [38]).
227 A preliminary sensitivity study was carried out considering the hygro-thermo-chemical model
228 applied to an exposed-exposed concrete component that highlighted the presence of two regions
229 where the humidity measurements presented the highest sensitivities, i.e. at the concrete mid-
230 height and a position close to the concrete surface (i.e. at about 10 mm from the external surface),
231 for the first few months from casting, while the highest sensitivity for the temperature

232 distributions are noted at the mid-height of the concrete component in the first 6 hours from
233 casting.
234 The sensitivity index is computed as partial derivative of the measured quantities, e.g. total
235 deformation ε, with respect to the model parameters p_i at a certain time instant *t* and in a certain
236 position *z* along the thickness of the concrete component as follows:

$$S_{\varepsilon,p_i}(z,t,\mathbf{p}) = \frac{\partial \varepsilon(\mathbf{p},z,t)}{\partial p_i} \frac{p_i}{\varepsilon(\mathbf{p},z,t)} \tag{9}$$

237 This index is normalised, for comparison purposes, with respect to both the parameter and the
238 measured quantity value. In the numerical computations, the derivatives have been approximated
239 by forward finite-differences with 0.1% increment, and have been evaluated at the top and
240 bottom surfaces of the concrete component and for a certain number of time instants.
241 Figure 6 shows the sensitivity index, continuously varying in time and space, computed
242 according to Equation (9), of the deformation profiles measured at the top and bottom surfaces
243 of both exposed-exposed and exposed-sealed concrete components. In particular, the sensitivity
244 index computed for the exposed-sealed (ES) concrete component appear to be generally higher
245 than those determined for the exposed-exposed (EE) case. Under the ES boundary condition, the
246 deformations measured at the sealed (bottom) surface generally show a higher sensitivity to the
247 model parameters than that of the deformation measured at the exposed (top) surface.
248 All parameters governing cement hydration, namely A_{c2}, η_c and γ_c, reach their highest
249 sensitivity on the measured deformation profiles after a few days from casting, when this
250 chemical reaction is more active, and the maximum value among these occurs for parameter γ_c
251 related to the hydration activation energy while sensitivity with respect to A_{c2} is almost
252 negligible. It is also interesting to observe that the sensitivity of the deformation profile,
253 measured at the sealed surface, with respect to the model parameters other than those governing
254 cement hydration, reaches always its highest value in the first few months after casting, therefore

highlighting how, during this period, the experimental information collected are mostly bound to enhance the identifiability of the sought parameters.

Among the parameters governing moisture permeability, the one which most affects the deformation profiles is the exponent *n*, characterized by a sensitivity index greater than the ones computed for parameters D_0 and D_1. Sensitivity with respect to Q_c is almost negligible since this parameter is expected to influence primarily the variation of the temperature field.

Figure 7 illustrates some representative sensitivity results obtained with respect to selected model parameters over a period of one year for concrete thicknesses of 100 mm and 250 mm. In particular, the thinner component exhibits an extremely high sensitivity for the deformation measured at its sealed (bottom) surface for about 30 days from casting, and the differences in sensitivity exhibited between the strains measured at the sealed (bottom) and exposed (top) sides of the thinner component are more pronounced than those calculated for the thicker component.

4. Inverse analysis

The inverse problem is usually formulated as the minimization of the discrepancy between the experimental results and same quantities numerically computed as a function of the sought parameters.

The identifiability of the parameters contained in the hygro-thermo-chemical-mechanical model presented in Section 2 has been investigated following a numerical procedure already adopted in other studies (see e.g. [39,40,41]), which consists of the implementation of different inverse analysis exercises starting from the so-called pseudo-experimental results, i.e. results numerically generated from a given set of model parameters, supplied in input to the inverse problem, which, if well-posed, should provide in output the values of the parameters adopted to generate the pseudo-experimental data.

The input data consist of humidity and temperature profiles taken at different locations through the concrete thickness and at different time instants as well as the total deformations measured

at both sides of the concrete component after completion of the curing period. In particular, the relative humidity $h_{e,\tau s}$ is measured through the concrete component thickness in a discretised number of locations $s = 1 \mathrm{K}\ N_{hz}$ and for a certain number of time instants $\tau = 1 \mathrm{K}\ N_{ht}$. Similarly, at each instant $\tau = 1 \mathrm{K}\ N_{Tt}$, the temperature distribution $T_{e,\tau s}$ is measured through the thickness of the component in a discretised number of points $s = 1 \mathrm{K}\ N_{Tz}$; and at each instant $\tau = 1 \mathrm{K}\ N_{\varepsilon t}$, total deformation $\varepsilon_{e,\tau s}$ is measured at the two sides (i.e. top and bottom) of the concrete component. The choice of the discretization points adopted for both the space and time domains is based on the outcomes of the sensitivity analysis.

In the present study all experimental information are processed together and uncertainties of both experimental measurements and system modelling are not considered within a stochastic framework, but the effect of random noise, applied to the inverse problem input data, is accounted for to investigate the robustness of the proposed identification procedure.

Collecting the model parameters to be estimated (i.e. those listed in the lower part of Table 1) in vector $\boldsymbol{p}$, and denoting experimental and computed quantities by subscripts "e" and "c", respectively, the discrepancy norm between measured and computed quantities can be expressed as follows:

$$w(\mathbf{p}) = \phi_h \sum_{\tau}^{N_{ht}} \sum_{s}^{N_{hz}} \left[\frac{\left(h_{n,\tau s} - h_{e,\tau s} \right)^2}{h_{e,\tau s}^2} \right] + \phi_T \sum_{\tau}^{N_{Tt}} \sum_{s}^{N_{Tz}} \left[\frac{\left(T_{n,\tau s} - T_{e,\tau s} \right)^2}{T_{e,\tau s}^2} \right] + \phi_\varepsilon \sum_{\tau}^{N_{\varepsilon t}} \sum_{s}^{2} \left[\frac{\left(\varepsilon_{n,\tau s} - \varepsilon_{e,\tau s} \right)^2}{\varepsilon_{e,\tau s}^2} \right] \qquad (10)$$

where $\phi_h = 1/(N_{ht} N_{hz})$, $\phi_T = 1/(N_{Tt} N_{Tz})$ and $\phi_\varepsilon = 1/(2 N_{\varepsilon t})$ are weight factors defined in order to ensure an equivalent contribution of the three terms defining the objective function.

The minimization of the objective function in Equation (10) is performed by the Trust Region (TR) algorithm (see, e.g. [42,43]). Starting from an assigned initialization vector, this is automatically updated by means of an iterative procedure based on the minimization of a quadratic approximation of the objective $w(\mathbf{p})$ within a "trust" region, whose dimensions are

updated step by step based on the results of the previous iteration. The process is stopped by the fulfilment of a priori tolerances on either the variation of the objective function or the Euclidean norm of the normalized optimization variables.

For each adopted set $\mathbf{p}^{ad}$ of the parameters model, pseudo-experimental data are generated and perturbated by different noise extractions $(n = 1...N_{NOISE})$, generated with uniform probability density over an interval centred on the exact value. For each noise extraction, the inverse problem is solved several times $(i = 1...N_{INIT})$ starting from different initialization vectors, to check the occurrence of local minima that might exist in view of the nonlinear and non-convex nature of the objective function. For a given noise extraction the identified value $\mathbf{p}_n^{id}$ is computed as average of all values $\mathbf{p}_{ni}^{id}$ identified in relation to the different initializations, weighted with respect to the inverse of the objective function in solution, as:

$$\mathbf{p}_n^{id} = \sum_i^{N_{INIT}} \mathbf{p}_{ni}^{id} \chi_i \Big/ \sum_i^{N_{INIT}} \chi_i \,, \quad \chi_i = 1 \Big/ w\left(\mathbf{p}_{ni}^{id}\right) \tag{11}$$

The identification error for each model parameter *k* is then computed as:

$$err_{n,k}^{id} = 100 \cdot \left| \frac{p_{n,k}^{id} - p_k^{ad}}{p_k^{ad}} \right| \tag{12}$$

A final measure of the identifiability error of each sought parameter is defined in terms of average of all the single errors, computed for each noise extraction:

$$err_k^{id} = \frac{1}{N_{NOISE}} \sum_n^{N_{NOISE}} err_{n,k}^{id} \tag{13}$$

with $err_{n,k}^{id}$ being defined as absolute value, see equation (12), to avoid compensations between errors of opposite signs when a large number of random noise extractions is adopted.

4.1 Results

Different inverse analysis exercises have been solved in the following to investigate the optimal formulation of the inverse problem for the full identification of the parameters listed in the lower

part of Table 1, i.e. those characterised by a large variability or not amenable to direct measurement for the lack of a precise physical meaning. As input data to the inverse problem, humidity, temperature and deformation profiles' measurements have been considered. In the following, only representative results are presented to outline and support the key findings of this work.

The concrete properties included in the simulations correspond to the mean values reported in Table 2 and those specified in Table 3. The external temperature has been assumed constant and equal to 20ºC. In all simulations, a random noise of 10% has been applied to the numerically generated pseudo-experimental data used in input.

The first inverse analysis simulations highlighted how the inverse problem is not well posed for the concurrent identification of parameters A_{c1} and γ_c. This lack of identifiability is attributed to the form in which these parameters appear in Equation (1) for the evaluation of the rate of cement hydration reaction $\dot{\alpha}$. In this equation, both parameters have an equivalent effect on $\dot{\alpha}$, i.e. an increase in A_{c1} leads to an increase of $\dot{\alpha}$ that could be similarly produced by a decrease of γ_c. Because of this, the inverse analysis procedure cannot distinguish between these two parameters and, in view of a much higher sensitivity of γ_c, the following inverse analysis exercises will be carried out assuming A_{c1} known a priori while still identifying γ_c. The validity of this assumption is later confirmed by the results outlining how the adoption of different a priori values for A_{c1} does not jeopardize the identifiability of the sought parameters.

Table 4 reports the results obtained considering a 100 mm thick concrete component wet cured for 1 day from casting, exposed to an ambient relative humidity equal to 40% and assuming different boundary conditions. The number of discrete humidity measurements through the thickness of the concrete component have been varied and the inclusion of a temperature measurement has been considered. The measurements are performed for a period of 30 days (with a frequency of one measurement per hour). Columns A, B, C and D in Table 4 provide the

results obtained under exposed-exposed (denoted as EE) conditions (Figure 1a) and highlight the need to use two relative humidity measurements (column D) to ensure the identifiability of all parameters (with identified errors' magnitude within the noise level introduced in the pseudo-experimental data). By using one relative humidity measurement, for example located at 50 mm (Column B) or 10 mm (Column C) from the external concrete surface, or without monitoring relative humidity (Column A), the information provided as input of the inverse problem is not sufficient for the identification of all sought parameters, because the estimation of D_0 or D_1 produces an error (at its maximum of 36.5%) that is larger than the magnitude of the added noise. For an exposed-sealed (referred to as ES) concrete component, column E shows that the experimental information consisting of one temperature and both surface deformation measurements are sufficient to guarantee the identifiability of all parameters. The inclusion of one relative humidity measurement for the ES conditions, for example located at the component mid-height, does not improve significantly the results as depicted by the values reported in column F of Table 4. Columns G and H highlight that, without the inclusion of a temperature measurement, the identification procedure does not lead to a successful characterisation of $Q_c^{\%}$ and A_{c2} when considering both EE and ES exposure conditions. These observations highlight how the use of a temperature measurement as experimental information is crucial for the identification of the model parameters governing cement hydration that cannot be identified if information on deformation or relative humidity only are considered.

The results discussed above have been obtained for a relatively thin concrete component with a thickness of 100 mm. In the case of a 250 mm thick component, representative errors are presented in Table 5. In this case, a longer period of measurements, of at least 60 days, is needed for the exposed-exposed case (as depicted in Columns B and C) to collect the amount of experimental information needed for the calibration of the model parameters, especially of those governing the moisture permeability. Shorter monitored periods (reported in column A for

372 30 days) do not provide sufficient experimental information for the identification. For an
373 exposed-sealed concrete component, differently from the 100 mm thickness, temperature and
374 deformation profiles are not sufficient for the present identification purposes (see columns D and
375 E), and one humidity measurement taken at mid-height is necessary to make the inverse problem
376 well posed (see columns F and G). This is here attributed to the fact that, as shown in Figure 7,
377 the sensitivity of the deformation measurements at the sealed concrete surface of a thicker
378 component is much lower than the corresponding value obtained for a thinner component. As a
379 consequence, the experimental information obtained from a thicker component is not sufficient
380 for the definition of a well-posed inverse problem without the use of humidity measurements.
381 This consideration is confirmed by the results reported in Table 6, where it is shown that for an
382 increasing concrete component thickness (varying from 100 mm to 400 mm in columns A to D),
383 the parameter κ_{vg}^{c} is identified with an increasing error. For the thicknesses considered in
384 columns B-D, it is necessary to include at least one relative humidity measurement, for example
385 placed at the concrete mid-height, to ensure the identifiability of all model parameters as depicted
386 in columns F-H.
387 At the beginning of this section, it has been discussed that the parameters A_{c1} and γ_c could not
388 be uniquely identified. For this reason, the inverse methodology followed in this study consisted
389 in assigning an a priori value to A_{c1} equal to its mean value reported in the literature (=29450 s^{-1}
390 based on the range provided in Table 2), i.e. the same value adopted in generating the pseudo-
391 experimental data. Table 7 reports the results of some inverse analysis exercises when an
392 incorrect value for A_{c1} (i.e. different from the one used for the generation of the pseudo-
393 experimental data) is specified in input of the inverse analysis. In particular, the upper and lower
394 limits of A_{c1} (as specified in Table 2) are used for the results reported in columns B and C
395 considering the EE conditions and in columns E and F for the ES conditions, while columns A
396 and D depict the errors determined using the exact value for A_{c1} (i.e. the value adopted to

generate pseudo-experimental data). These results confirm that the identifiability of all parameters is not affected by an incorrect assumption of A_{c1}, except for the "companion" parameter γ_c, whose identification error increases, especially when the lower limit is assumed (however always within the order of magnitude of the added noise for the cases considered).

The inverse analysis cases proposed for the exposed-exposed and exposed-sealed conditions are revisited in the following assuming sinusoidal time-varying boundary conditions expressed in terms of external temperature and relative humidity applied to the concrete surfaces. Only selected case studies (taken from Tables 4 and 5) are considered in the following with the sinusoidal boundary conditions. In particular, columns A and C in Table 8 correspond to columns E and D in Table 4, respectively; while columns D and E correspond to columns B and F in Table 5, respectively. Based on these results, the optimal (in terms of minimum measurements to be taken) experimental setups studied for the 250 mm thick concrete component under external constant boundary conditions (Table 5) are still effective for the identification of the sought material parameters in the case of sinusoidally-varying boundary conditions, see columns D and E in Table 8. For the thinner specimen, some problems arise (with the varying boundary conditions) in relation to the identification of the parameter A_{c2}. In particular, column A in Table 8 shows that for the case of the exposed-sealed specimen the error increases (when compared to the case with constant boundary conditions) but it remains of the same order and magnitude of the added noise. It has been observed that this error can be further reduced by adding a temperature measurement close to the external surface (see column B in Table 8). The combination of the small thickness and of the exposed-exposed boundary conditions maximizes the influence of the time-varying boundary conditions on the measurements taken inside the specimen and induces the largest identification error of the parameter A_{c2}, as reported in column C (Table 8), however, without jeopardizing the identification of the other parameters.

5. Conclusions

This paper has focussed on the identifiability of the parameters required for a hygro-thermo-chemical-mechanical model that predicts variations of temperature, relative humidity and shrinkage induced deformations in concrete components. In particular, the model parameters have been subdivided into two main sets: (i) one set of parameters that can be evaluated on the basis of the concrete mix specifications or from literature data; and (ii) a second set of parameters that are characterised by a large variability and, in some cases, without a precise physical meaning, are not amenable to a direct measurement. This paper has proposed an inverse analysis procedure for the identification of the model parameters contained in this second set by considering different concrete exposure conditions and by using following variables as input data: total deformations at the concrete surfaces, temperature and relative humidity profiles in some positions inside the concrete component. These results may find applications in enhancing the design of in-situ investigations and of experimental tests, and in minimising the necessary collected experimental information (in terms of monitored period and number of discrete temperature and relative humidity measurements). The outcomes of the different inverse analyses' exercises have been considered successful when all parameters have been identified with an error smaller than the noise added to the pseudo-experimental data in input to the inverse problem. The boundary conditions included in this study are described as follows: (i) heat transfer has been assumed to take place through both concrete surfaces; and (ii) two exposure conditions have been considered for the relative humidity, i.e. one assuming both concrete surfaces to be exposed for drying (referred to as EE) and one where only one surface has been exposed with the remaining one being sealed (denoted as ES). The identification process has been applied considering different environments of external temperature and relative humidity surrounding the concrete.

Based on the results and case studies considered in this paper, it is possible to draw the conclusions listed below.

- For concrete components, subjected to constant boundary conditions (i.e. constant external temperature and relative humidity) and exposed on both sides (EE conditions), the minimum measurements required for the identification of all model parameters consist of relative humidities taken at two locations within the concrete thickness (e.g. one at the mid-height and one close to the surface), one temperature reading at mid-height and total deformation at the concrete surface.
- Concrete components, exposed to constant environmental conditions, sealed on one side and allowed to dry on the opposite one (ES conditions) require varying strategies depending on their thickness. For thinner components (here taken as 100 mm thick), all model parameters are identifiable by monitoring the total deformations at both the concrete surfaces and temperature at mid-height. For larger components, additional measurements related to relative humidity need to be included in the input data of the inverse analysis procedure.
- For concrete components exposed to sinusoidally-varying environmental conditions (i.e. varying external temperature and relative humidity), the inverse analysis requires the use of the measured external temperature and relative humidity variations as input data of the direct operator. It has been observed that for relatively large concrete thicknesses (here taken as 250 mm), the same minimum experimental information required for a concrete specimen exposed to constant boundary conditions is sufficient for the identification of the sought material parameters, while for thinner concrete components (here taken as 100 mm) the use of the same approach leads to larger error for only one parameter (associated with the variation of the degree of cement hydration over time) without jeopardizing the identification of the remaining parameters.

6. Acknowledgements

The work in this article was supported under the Australian Research Council's Discovery Projects funding scheme (project number DP140400529).

Appendix A

Matrices and vectors of the system in equation (8) are defined as follows:

$$\mathbf{W} = \bigcup_e \int_{\Omega_e} \mathbf{N}_e^T \frac{\partial w_e}{\partial h} \mathbf{N}_e \mathrm{d}\Omega \tag{A1}$$

$$\mathbf{D} = \bigcup_e \int_{\Omega_e} \mathbf{B}_e^T D_h \mathbf{B}_e \mathrm{d}\Omega \tag{A2}$$

$$\mathbf{F} = -\bigcup_e \int_{\Gamma_e} \mathbf{N}_e^T \mathbf{n}^T \mathbf{j} \mathrm{d}\Gamma - \bigcup_e \int_{\Omega_e} \mathbf{N}_e^T \left(\frac{\partial w_e}{\partial \alpha_c} + \frac{\partial w_n}{\partial \alpha_c} \right) \dot{\alpha}_c \mathrm{d}\Omega \tag{A3}$$

$$\mathbf{C} = \bigcup_e \int_{\Omega_e} \mathbf{N}_e^T \rho c_t \mathbf{N}_e \mathrm{d}\Omega \tag{A4}$$

$$\mathbf{\Lambda} = \bigcup_e \int_{\Omega_e} \mathbf{B}_e^T \lambda \mathbf{B}_e \mathrm{d}\Omega \tag{A5}$$

$$\mathbf{Q} = -\bigcup_e \int_{\Gamma_e} \mathbf{N}_e^T \mathbf{n}^T \mathbf{q} \, \mathrm{d}\Gamma + \bigcup_e \int_{\Omega_e} \mathbf{N}_e^T \dot{Q}_c \mathrm{d}\Omega \tag{A6}$$

where symbol $\bigcup_e$ refers to the assembly operation typical of the finite element approach, and matrices $\mathbf{N}_e$ and $\mathbf{B}_e$ collect shape functions and their spatial derivatives, respectively.

References

[1] Z.P. Bažant, L.J. Najjar, Nonlinear water diffusion in nonsaturated concrete, Materiaux et Constructions 5 (1972) 3–20.

[2] F.J. Ulm, O. Coussy, Modeling of thermo-chemical–mechanical couplings of concrete at early age, Journal of Engineering Mechanics ASCE 121 (1995) 785–794.

[3] M. Cervera, J. Oliver, T. Prato, Thermo–chemo–mechanical model for concrete. I: hydration and aging, Journal of Engineering Mechanics ASCE 125 (1999) 1018–1027.

[4] D. Gawin, F. Pesavento, B.A. Schrefler, Hygro-thermo-chemo-mechanical modelling of concrete at early ages and beyond, Part I: hydration and hygrothermal phenomena, International Journal Numerical Methods Engineering 67 (2006) 299–331.

[5] M. Du, X. Jin, H. Ye, N. Jin, Y. Tian, A coupled hygro-thermal model of early-age concrete based on micro-pore structure evolution, Construction and Building Materials 111 (2016) 689–698.

[6] T. Gasch, R. Malm, A. Ansell, A coupled hygro-thermo-mechanical model for concrete subjected to variable environmental conditions, International Journal of Solids and Structures 91 (2016) 143–156.

[7] J.K. Kim, C.S. Lee, Moisture diffusion of concrete considering self-desiccation at early ages, Cement and Concrete Research 29 (1999) 1921–1927.

[8] B.H. Oh, S.W. Cha, Nonlinear analysis of temperature and moisture distributions in early-age concrete structures based on degree of hydration, ACI Materials Journal 100 (2003) 361–70.

[9] S. Rahimi-Aghdama, Z.P. Bažant, M.J. Abdolhosseini Qomic, Cement hydration from hours to centuries controlled by diffusion through barrier shells of C-S-H, Journal of the Mechanics and Physics of Solids 99 (2017) 211–224.

501 [10] S.D. Abyaneh, H.S. Wong, N.R. Buenfeld, Modelling the diffusivity of mortar and concrete
502 using a three-dimensional mesostructure with several aggregate shapes, Computational Materials
503 Science 78 (2013) 63–73.

504 [11] S.D. Abyaneh, H.S. Wong, N.R. Buenfeld, Simulating the effect of microcracks on the
505 diffusivity and permeability of concrete using a three-dimensional model, Computational
506 Materials Science 119 (2016) 130–143.

507 [12] S.B. Tang, Q.L. Yu, H. Li, C.Y. Yu, C.Y. Bao, C.A. Tang, Mesomechanical model of
508 moisture diffusion and shrinkage cracking in building material – Model development,
509 Construction and Building Materials 47 (2013) 511–529.

510 [13] G. Di Luzio, G. Cusatis, Hygro-thermo-chemical modeling of high performance concrete.
511 I: Theory, Cement & Concrete Composites 31 (2009) 301–308.

512 [14] G. Di Luzio, G. Cusatis, Hygro-thermo-chemical modeling of high performance concrete.
513 II: Numerical implementation, calibration, and validation, Cement & Concrete Composites 31
514 (2009) 309–324.

515 [15] P. Havlásek, M. Jirásek, Multiscale modeling of drying shrinkage and creep of concrete,
516 Cement and Concrete Research 85 (2016) 55–74.

517 [16] F.H. Wittmann, Creep and shrinkage mechanics, in: Z.P. Bažant, F.H. Wittmann (Eds.),
518 Creep and Shrinkage of Concrete Structures, John Wiley & Sons Ltd., 1982, pp. 129–161.

519 [17] ACI (2006) ACI 302.2R-06 Guide for Concrete Slabs that Receive moisture-sensitive
520 flooring materials, American Concrete Institute.

521 [18] H.J. Oh, Y.K Cho, Y. Seo, S.-M. Kim, Experimental analysis of curling behaviour of
522 continuously reinforced concrete pavement, Construction and Building Materials 128 (2016) 57–
523 66.

524 [19] G. Ranzi, G. Leoni, R. Zandonini, State of the art on the time-dependent behaviour of
525 composite steel-concrete structures, Journal of Constructional Steel Research 80 (2013) 252–
526 263.
527 [20] G. Ranzi, Service design approach for composite steel-concrete floors, Proceedings of the
528 Institution of Civil Engineers: Structures and Buildings, https://doi.org/10.1680/jstbu.16.00196.
529 [21] Q. Wang, G. Ranzi, Y. Wang, Y. Geng, Long-term behaviour of simply-supported steel-
530 bars truss slabs with recycled coarse aggregate, Construction and Building Materials 116 (2016)
531 335–346.
532 [22] R.I. Gilbert, M.A. Bradford, A. Gholamhoseini, Z.-T. Chang, Effects of Shrinkage on the
533 Long-Term Stresses and Deformations of Composite Concrete Slabs, Engineering Structures 40
534 (2012) 9–19.
535 [23] H.D. Bui, Inverse Problems in the Mechanics of Materials: an Introduction, CRC Press,
536 Boca Raton FL, 1994.
537 [24] Z. Mroz, G.E. Stavroulakis, Identification of Materials and Structures, CISM Lecture Notes,
538 Vol. 469, Springer-Verlag, Wien, 2005.
539 [25] G. Stavroulakis, G. Bolzon, Z. Waszczyszyn, L. Ziemianski, Inverse analysis, in: B.
540 Karihaloo, R.O. Ritchie, I. Milne (Eds.), Comprehensive Structural Integrity, Elsevier Science
541 Ltd., Kidlington (Oxfordshire), UK, 2003.
542 [26] S.J. Pantazopoulo, R.H Mills, Microstructural aspects of the mechanical response of plain
543 concrete, ACI Materials Journal 92 (1995) 605–616.
544 [27] M. Jooss, H.W. Reinhardt, Permeability and diffusivity of concrete as function of
545 temperature, Cement Concrete Research 32 (2002) 1497–1504.
546 [28] F. Benboudjema, F. Meftah, J.M. Torrenti, Interaction between drying, shrinkage, creep and
547 cracking phenomena in concrete, Engineering Structures 27 (2005) 239–250.

548 [29] M. Jirásek, P. Havláseka, Microprestress–solidification theory of concrete creep:
549 Reformulation and improvement, Cement and Concrete Research 60 (2014) 51–62.

550 [30] M. Azenha, C. Sousa, R. Faria, A. Neves, Thermo–hygro–mechanical modelling of self-
551 induced stresses during the service life of RC structures, Engineering Structures 33 (2011) 3442–
552 3453.

553 [31] G. Di Luzio, G. Cusatis, Solidification–microprestress–microplane (SMM) theory for
554 concrete at early age: Theory, validation and application, International Journal of Solids and
555 Structures 50 (2013) 957–975.

556 [32] L. Wan, R. Wendner, B. Liang, G. Cusatis, Analysis of the behavior of ultra high
557 performance concrete at early age, Cement and Concrete Composites 74 (2016) 120–135.

558 [33] A. Quarteroni, Modellistica numerica per problemi differenziali, Springer-Verlag Italia,
559 Milano, 2000.

560 [34] R. D. Cook, D. S. Malkus, M. E. Plesha, R. J. Witt, Concepts and applications of finite
561 element analysis, 4th Edition, Wiley, 2002.

562 [35] R.I. Gilbert, G. Ranzi, Time-dependent behaviour of concrete structures, Spon Press,
563 London, UK, 2011.

564 [36] EN 1992-1-1, Eurocode 2: Design of concrete structures - Part 1-1: General rules and rules
565 for buildings, European Committee for Standardization, 2004.

566 [37] AS3600, Australian Standard for Concrete Structures AS3600–2009, Standards Australia,
567 2009.

568 [38] M. Kleiber, H. Antúnez, T.D. Hien, P. Kowalczyk, Parameter Sensitivity in Nonlinear
569 Mechanics, Theory and Finite Element Computations, John Wiley & Sons, Chichester, 1997.

570 [39]. M. Bocciarelli, V. Buljak, C.K.S. Moy, S.P. Ringer, G. Ranzi, An inverse analysis approach
571 based on a POD direct model for the mechanical characterization of metallic materials,
572 Computational Materials Science 95 (2014) 302–308.
573 [40] G. Bolzon, M. Talassi, An effective inverse analysis tool for parameter identification of
574 anisotropic material models, International Journal of Mechanical Sciences 77 (2013) 130–144.
575 [41] R. Ardito, G. Cocchetti, Statistical approach to damage diagnosis of concrete dams by radar
576 monitoring: Formulation and a pseudo-experimental test, Engineering Structures 28 (2006)
577 2036–2045.
578 [42] T.F. Coleman, Y. Li, SIAM Journal of Optimization 6 (1996) 418–445.
579 [43] The Math Works Inc, USA, User's Guide and Optimization Toolbox, Release 6.13, Matlab
580 2004.
581

582 Table 1. Material parameters required in input
583 of the hygro-thermo-chemical-mechanical model.

	Parameter	Description
Parameters calculated based on concrete mix specifications or assigned known values well accepted in the literature	c	cement content
	w/c	water-to-cement ratio
	a,b	parameters associated with the variation of the degree of cement hydration over time and taken as a = 7.5 and b = 4.0 [1]
	λ	heat conductivity
	ρ	concrete mass density
	c_t	concrete specific heat
	k_c	parameter associated with non-evaporable water and taken as 0.253 (as suggested in [13])
Parameters characterised by a large variability (see Table 2) – some of which do not possess a precise physical meaning (to be identified with the inverse analysis presented in Section 4)	A_{c1}, A_{c2}, η_c	parameters with no precise physical meaning associated with the variation of the degree of cement hydration over time
	γ_c	parameter calculated as the ratio of the hydration activation energy over the universal gas constant
	Q_c^∞	total heat content per unit cement mass due to cement hydration
	κ_{vg}^c	parameter that governs the amount of water contained in the cement gel pores
	g_1	parameter that governs the shape of the sorption curve
	D_0, D_1, n	parameters that control the moisture permeability and depend on the specific concrete mix
	k_{sh}	parameter that relates the change over time of the free shrinkage deformation to the rate of the relative humidity

584

585

586 Table 2. Range of variation for the parameters listed in the lower part of Table 1.

Parameter	Range of variation	Mean value
A_{c1}	3900 – 55000 [s^{-1}]	29450
A_{c2}	10^{-6} – $5\cdot10^{-2}$	$2.5\cdot10^{-2}$
η_c	5.5 – 8.0	6.75
γ_c	3000 – 8000 [K]	5500
Q_c^0	400 – 550 [kJ/kg]	475000
κ_{vg}^c	0.10 – 0.26	0.18
g_1	1.20 – 2.20	1.70
D_0/c	$0.2\cdot10^{-14}$ – $7.5\cdot10^{-14}$ [m^2/s]	$3.85\cdot10^{-14}$
D_1/c	$4.8\cdot10^{-10}$ – $12\cdot10^{-10}$ [m^2/s]	$8.4\cdot10^{-10}$
n	3.0 – 4.5	3.75
k_{sh}	5×10^{-4} – 3.5×10^{-3}	2.0×10^{-3}

587

588

589 Table 3. Specifications of the concrete mix and some parameters used in the numerical
590 simulations.

Parameter	Assumed value
c	312 kg/m^3
w/c	0.57
λ	2.3 W/mºC
ρ	2400 kg/m^3
c_t	1100 J/kgºC
k_c	0.253

591

592

593

594

Table 4. Results of the inverse analysis exercises in terms of err_k^{id} [%] by varying: boundary conditions and location of discrete measurements for the relative humidity *h* and the temperature *T*.

D	100 mm							
RH	40%							
Period of wet curing	1 day							
Period monitored	30 days							
Added noise	10%							
Boundary conditions	EE				ES		EE	ES
Location of discrete measurements[1] for *h* [mm]	/	50	10	50/10	/	50	50/10	50/10
Location of discrete measurements[1] for *T* [mm]	50				50		/	/
Column	A	B	C	D	E	F	G	H
D_0	8.5	36.5	10.6	8.7	4.1	2.3	2.7	2.0
D_1	13.7	5.9	4.8	6.4	1.9	1.3	2.1	0.8
n	2.8	4.4	0.9	0.7	0.4	0.5	0.4	0.3
κ_{vg}^c	8.0	8.8	6.8	9.6	3.1	3.9	4.6	3.7
g_1	7.2	5.0	5.2	8.2	1.4	0.6	3.0	1.1
γ_c	0.1	0.1	0.1	0.1	0.2	0.2	0.2	0.6
Q_c^*	6.1	3.7	3.7	4.2	1.9	1.2	13.3	6.8
A_{c2}	8.2	5.3	6.2	8.1	3.8	2.8	4.9	12.2
η_c	8.9	5.2	5.1	6.1	2.6	1.6	2.4	0.9
k_{SH}	8.0	2.2	0.6	0.6	1.3	0.3	0.3	1.2

NOTE: [1]Locations measured from external surfaces of concrete component [mm].

Table 5. Results of the inverse analysis exercises in terms of err_k^{id} [%] by varying: boundary conditions, location of discrete measurements for the relative humidity *h* and period monitored.

D	250 mm						
Location of discrete measurements for *T*	125 mm						
RH	40%						
Period of wet curing	1 day						
Added noise	10%						
Boundary conditions	EE			ES			
Location of discrete measurements for *h* [mm]	125/10			/		125	
Period monitored [days]	30	60	90	60	90	60	90
Column	A	B	C	D	E	F	G
D_0	14.5	6.1	2.3	5.3	8.1	6.8	4.8
D_1	3.0	1.8	2.4	2.4	3.5	3.2	3.1
n	2.2	1.0	0.4	0.9	1.2	1.1	0.8
κ_{vg}^c	10.3	6.0	6.2	11.8	19.0	8.2	7.1
g_1	3.5	1.8	2.3	2.6	5.3	2.3	1.9
γ_c	0.1	0.1	0.1	0.2	0.2	0.1	0.2
Q_c^∞	1.4	1.0	1.2	0.7	1.7	0.8	1.1
A_{c2}	2.8	3.3	4.5	6.2	4.6	4.7	4.8
η_c	1.7	1.0	1.0	1.7	2.0	1.5	0.8
k_{SH}	0.5	0.2	0.2	1.3	2.2	0.2	0.2

NOTE: [1]Locations measured from external surfaces of concrete component [mm].

610 Table 6. Results of the inverse analysis exercises in terms of err_k^{id} [%] for an exposed-sealed
611 specimen by varying: location of discrete measurements for the relative humidity *h* and
612 component thickness D.

Location of discrete measurements for *T*	0.5×D							
RH	40%							
Period of wet curing	1 day							
Period monitored	90 days							
Added noise	10%							
Boundary conditions	ES				ES			
Location of discrete measurements for *h* [mm]	/				0.5×D			
D [mm]	100	200	300	400	100	200	300	400
Column	A	B	C	D	E	F	G	H
D_0	3.2	5.8	7.2	8.4	4.9	3.0	6.6	6.8
D_1	1.7	1.9	2.9	6.4	1.6	2.1	3.5	5.2
n	0.4	0.7	1.0	1.4	0.3	0.5	1.0	1.1
κ_{vg}^{c}	5.3	14.3	18.6	20.5	5.1	6.0	7.5	9.4
g_1	1.2	3.5	5.3	5.9	1.6	1.5	2.0	2.7
γ_c	0.1	0.2	0.2	0.2	0.1	0.2	0.2	0.2
Q_c^0	1.0	1.5	1.5	1.4	0.9	1.1	1.1	1.1
A_{c2}	2.5	4.2	5.5	5.8	2.9	4.1	5.3	5.8
η_c	1.6	1.6	1.5	1.5	1.3	0.8	0.8	0.8
k_{SH}	0.7	1.7	2.2	1.8	0.2	0.2	0.2	0.3

613 NOTE: [1]Locations measured from external surfaces of concrete component [mm].

614

615

Table 7. Results of the inverse analysis exercises in terms of err_k^{id} [%] by varying: boundary conditions, location of discrete measurements for the relative humidity *h* and assuming different a-priori values for the parameter A_{c1}.

D	100 mm					
Location of discrete measurements for *T*	50 mm					
RH	40%					
Period of wet curing	1 day					
Period monitored	30 days					
Added noise	10%					
Boundary conditions	EE			ES		
Location of discrete measurements[1] for *h* [mm]	50/10			50		
Parameter A_{c1} [s^{-1}]	29450	3900	55000	29450	3900	55000
Column	A	B	C	D	E	F
D_0	8.7	9.0	9.0	2.3	3.4	2.4
D_1	6.4	5.6	5.5	1.3	0.8	1.3
n	0.7	0.6	0.6	0.5	0.3	0.6
κ_{vg}^c	9.6	6.1	6.1	3.9	2.8	4.1
g_1	8.2	7.1	7.0	0.6	0.9	0.6
γ_c	0.1	10.8	3.3	0.2	10.5	3.4
Q_c^∞	4.2	4.5	4.4	1.2	0.8	1.1
A_{c2}	8.1	7.2	7.0	2.8	1.5	3.2
η_c	6.1	6.8	6.7	1.6	1.2	1.6
k_{SH}	0.6	0.3	0.3	0.3	0.4	0.5

NOTE: [1]Locations measured from external surfaces of concrete component [mm].

Table 8. Results of the inverse analysis exercises in terms of err_k^{id} [%] by considering sinusoidal time-varying boundary conditions, in terms of external temperature and relative humidity.

RH	40%±10%				
Temperature	20°±5°				
Period of wet curing	1 day				
Added noise	10%				
Concrete thickness D [mm]	100			250	
Period monitored [days]	30			60	
Boundary conditions	ES	ES	EE	EE	ES
Location of discrete measurements for h [mm]	/	/	50/10	125/10	125
Location of discrete measurements for T [mm]	50	50/5	50	125	125
Column	A	B	C	D	E
D_0	1.8	2.7	1.6	5.6	3.5
D_1	1.2	1.3	5.4	2.4	2.7
n	0.8	0.7	0.6	1.0	0.4
κ_{vg}^c	1.9	1.2	7.2	4.0	3.5
g_1	0.9	0.6	5.4	1.5	0.8
γ_c	1.2	1.5	1.3	0.3	0.2
Q_c^0	4.6	4.0	7.0	0.9	1.0
A_{c2}	11.5	9.3	23.1	9.5	9.7
η_c	1.6	1.9	2.7	0.9	1.2
k_{SH}	2.2	2.3	0.4	0.5	0.4

628

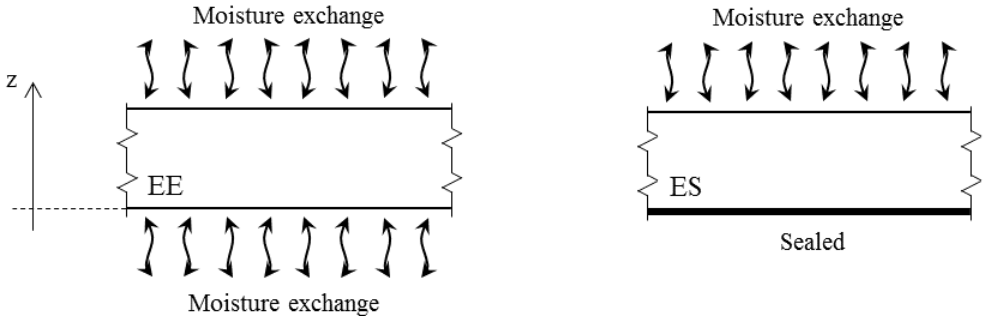

629

630 (a) Exposed-exposed conditions (EE) (b) Exposed-sealed conditions (ES)

631 Figure 1. Boundary conditions considered for the relative humidity field.

632

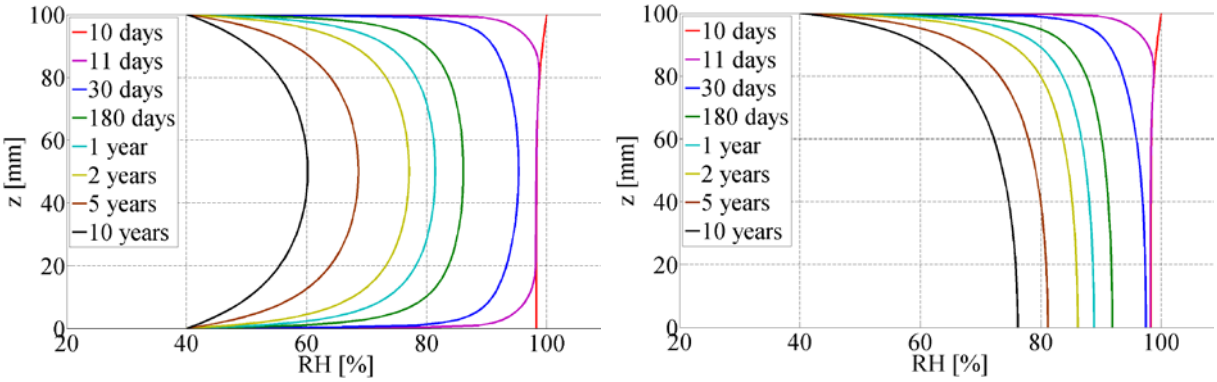

(a) EE boundary condition (Figure 1a). (b) ES boundary condition (Figure 1b).

Figure 2. Relative humidity (RH) profiles for 10 years of simulation under different exposure conditions for a 100 mm thick concrete component exposed to environmental RH of 40%.

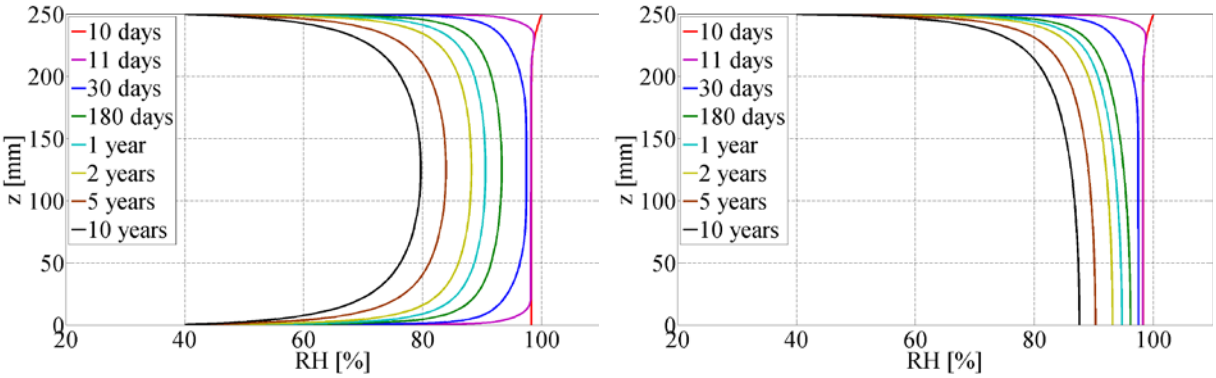

(a) EE boundary condition (Figure 1a). (b) ES boundary condition (Figure 1b).

Figure 3. Relative humidity (RH) profiles for 10 years of simulation under different exposure conditions for a 250 mm thick concrete component exposed to environmental RH of 40%.

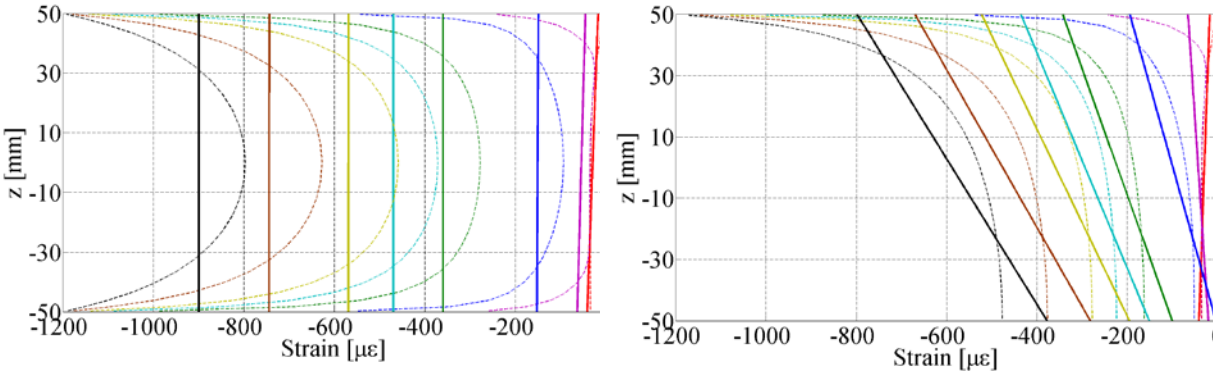

(a) EE boundary condition (Figure 1a).

(b) ES boundary condition (Figure 1b).

Figure 4. Total deformations (continuous lines) and free shrinkage deformations (dotted lines) for 10 years of simulation (at same instants in time of Figure 2) under different exposure conditions over a 100 mm concrete thickness exposed to environmental RH of 40%.

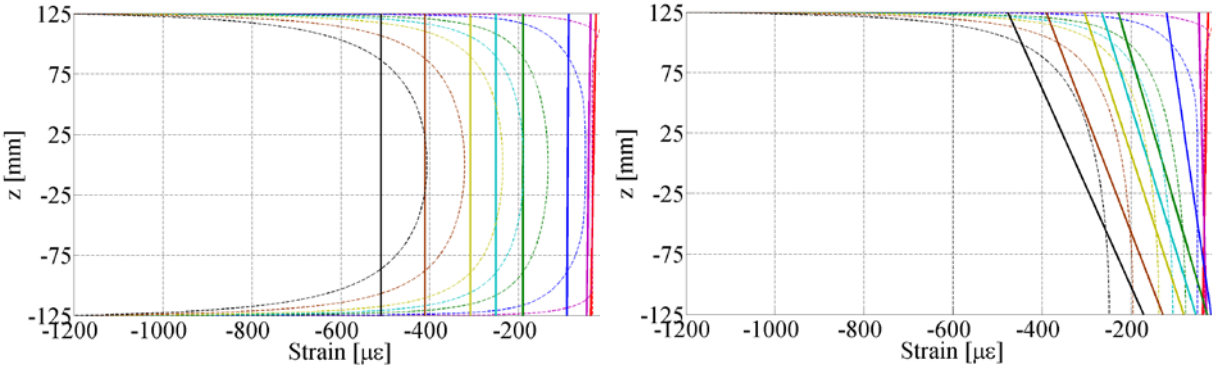

(a) EE boundary condition (Figure 1a). (b) ES boundary condition (Figure 1b).

643 Figure 5. Total deformations (continuous lines) and free shrinkage deformations (dotted lines)
644 for 10 years of simulation (at same instants in time of Figure 3) under different exposure
645 conditions over a 250 mm concrete thickness exposed to environmental RH of 40%.
646

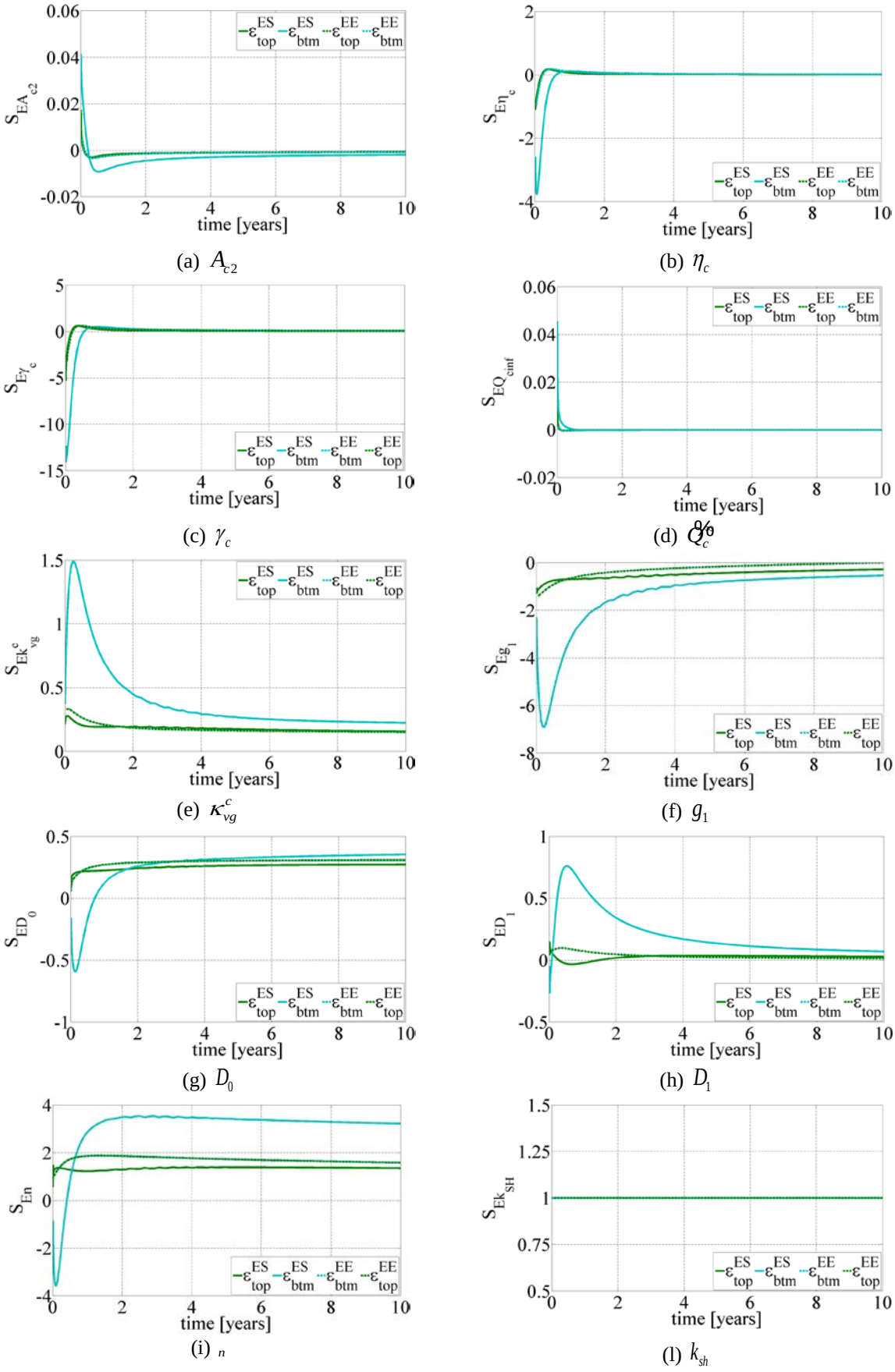

Figure 6. Sensitivity of deformation measurements with respect to the model parameters for a 250 mm thick concrete component and an external humidity of 40 %.

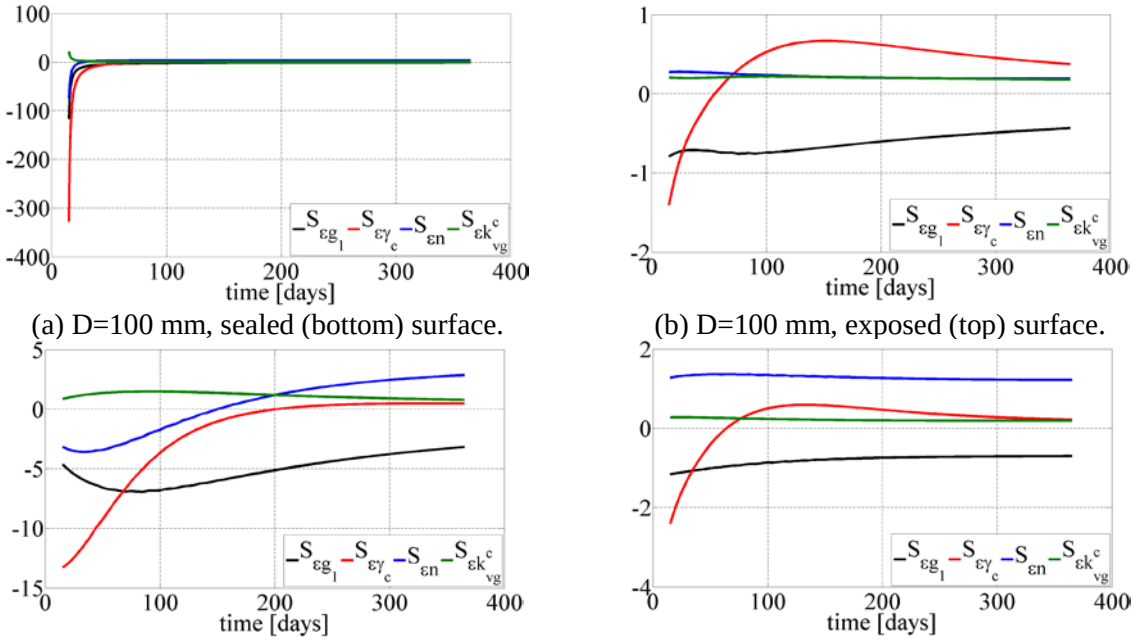

(a) D=100 mm, sealed (bottom) surface.

(b) D=100 mm, exposed (top) surface.

(c) D=250 mm, sealed (bottom) surface.

(d) D=250 mm, exposed (top) surface.

Figure 7. Sensitivity of deformation measurements with respect to selected model parameters for thicknesses of 100 mm and 250 mm, and external humidity of 40%.